Catalysis Science & Technology

Continuous Hydroxyketone Production from Furfural Using Pd-TiO2 Supported on Activated Carbon

Journal:	*Catalysis Science & Technology*
Manuscript ID	CY-ART-08-2020-001556.R1
Article Type:	Paper
Date Submitted by the Author:	11-Aug-2020
Complete List of Authors:	Kastner, James; The University of Georgia, Biochemical Engineering Pirmoradi, Maryam ; The University of Georgia, Biochemical Engineering Gulotty Jr., Robert ; Applied Catalysts

Continuous Hydroxyketone Production from Furfural Using Pd-TiO_2 Supported on Activated Carbon

Maryam Pirmoradi[1], Robert J. GulottyJr.[2], James R. Kastner[1]*

[1]Biochemical Engineering, College of Engineering Driftmier Engineering Center, The University of Georgia, 597 D.W. Brooks Drive, Athens, Georgia 30602, United States

e-mails: jkastner@engr.uga.edu
pirmoradi@uga.edu

[2]Applied Catalysts/Applied Ceramics Inc., 2 Technology Place
Laurens, SC 29360, Ph: 864-682-2597 x2916
bob.gulotty@appliedcatalysts.com

Abstract

Pd-TiO_2, Pd-Cu and Pd-Fe activated carbon (AC) supported catalysts were employed for continuous selective hydrogenation of furfural. Effect of reaction parameters on product selectivity and space time yield (STY) was determined. Weak acid sites, generated by Pd-TiO_2 catalyst opened the furan ring and resulted in a STY of 134 g/Lcat/h (610 g/kg-cat/h) and 39% selectivity of 5-hydroxy-2-pentanone (5H2P), a hydrogenation product of furan ring opening, in a short residence time (7.6 min) at 180 °C and 300 psig. The Pd-Cu and Pd-Fe catalysts were selective towards tetrahydrofurfuryl alcohol and furfuryl alcohol. A STY of 259 g/Lcat/h (1182 g/kg-cat/h) and 42% selectivity of furfuryl alcohol was achieved in presence of Pd-Cu catalyst at 180 °C and 300 psig (3.8 min). The Pd/TiO_2/AC catalyst shows promise for continuous production of 5H2P, a building block for many drugs and precursor to 1,4-pentanediol.

Keywords: Furfural, continuous, hydrogenation, activated carbon, metal-weak acid sites, 5-hydroxy-2-pentanone (3-acetyl-1-propanol)

Introduction

Furfural is an inexpensive, abundant, and biomass-derived aldehyde of furan. Hydrogenation of this chemical results in multiple value-added products such as furfuryl alcohol (FA), tetrahydrofurfuryl alcohol (THFA), 2-methylfuran (2MF) and 2-methyltetrahydrofuran (2MTHF).[1] FA is obtained from furfural through one step hydrogenation of the aldehyde group to alcohol. Hydrogen can further attack the formed alcohol group and result in 2MF through elimination of a water molecule. THFA can also be achieved through hydrogenation of FA ring double bonds. Cyclopentanone (CP) and 5-hydroxy-2-pentanone (5H2P) are two other valuable products of furfural hydrogenation. CP is a precursor for production of jet fuels, rubber chemicals and pharmaceuticals.[2] 5H2P works as an important ketone building block in synthesis of multiple medications; e.g., it's used as a component in the production of hydroxychloroquine and chloroquine.[3,4] Interestingly, the ketone building block for hydroxychloroquine (HCQ) and chloroquine (CQ) has been identified as a production bottleneck and is currently produced from petroleum based chloroalkynes, enol ethers, lactones, or chloroalkenes.[4] Several new HCQ and CQ synthesis pathways using 5H2P have been proposed.[4] With one further hydrogenation step of 5H2P, 1,4-pentanediol, an important linear diol for controlled drug delivery, cosmetics industry and polymer fabrication, is achieved.[5, 6] Obtaining CP requires a ring rearrangement step of FA's furan ring (known as Piancattelli rearrangement).[7] This step involves opening of the furan ring into an unstable intermediate in presence of a weak Lewis acid site and rearranging to 4-hydroxy-2-cyclopentenone (4HCP).[8] It has been previously reported that using water as a reaction solvent can promote the furfural ring rearrangement/opening step since water can act as a donor of H^+.[8, 9] Further hydrogenation steps of 4HCP result in CP. On the other hand, during furfural hydrogenation in presence of an acid catalyst, the formed unstable intermediate from ring opening step can undergo hydrogenation at the C=C bond to form 4-oxopentanal, a linear product, where a further hydrogenation step can result in 5H2P **(Figure 1**).[3] Therefore, the unstable intermediate compound will not undergo cyclization and ring rearrangement does not happen.

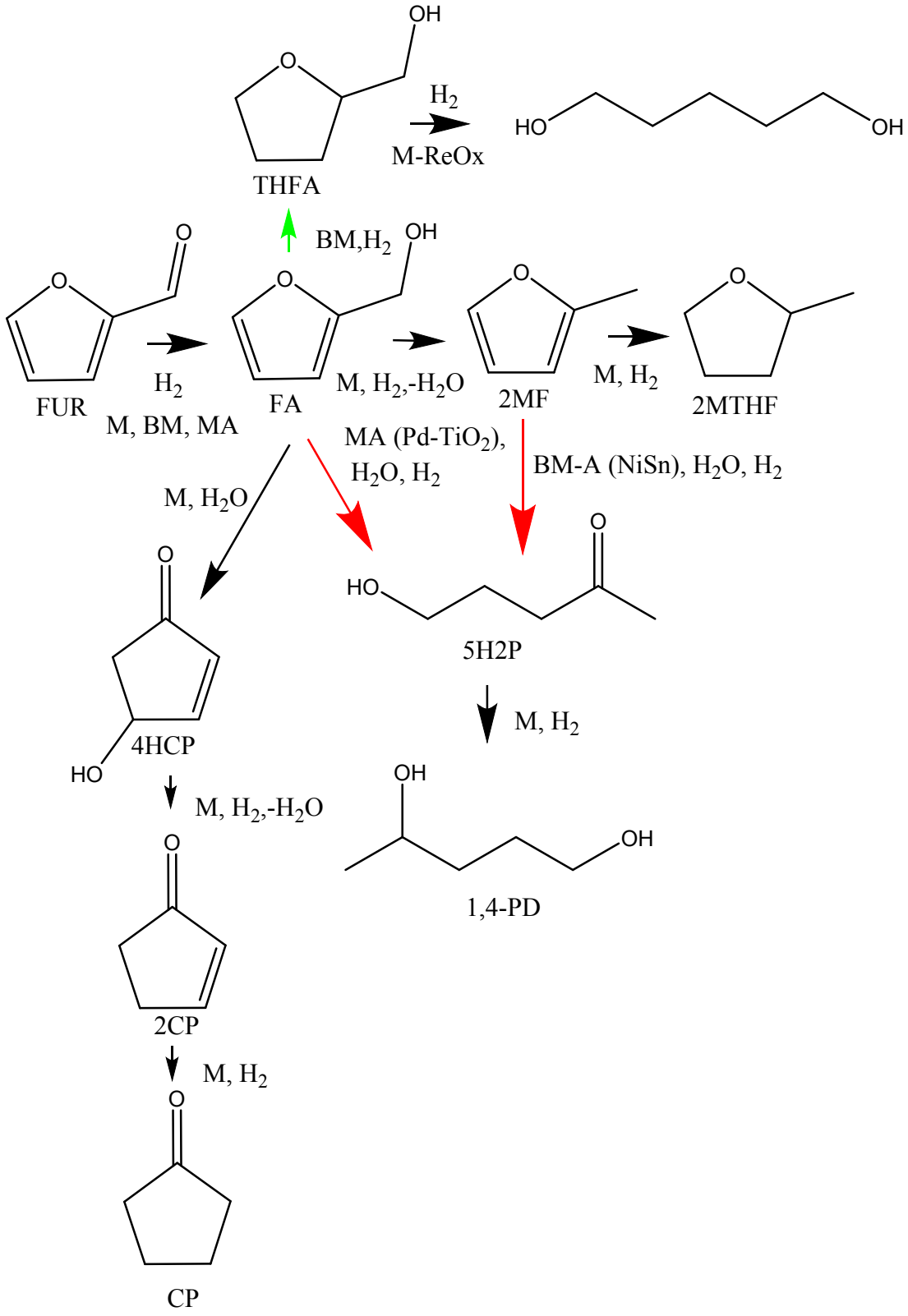

Figure 1. Hydrogenation, rearrangement, and ring opening pathways of furfuryl alcohol (FA) in presence of hydrogen and catalysts (M is metal such as Pd or Cu; BM is bi-metal such as Pd-Fe; MA is metal-acid such as Pd-TiO_2; BM-A is bimetal-acid; FUR, furfural; THFA, tetrahydrofurfuryl alcohol; 2MF, 2-methyl furan; 2MTHF, 2-methyltetrahydrofuran; 4HCP, 4-hydroxy-2-cyclopentenone; 2CP, 2-cyclopenten-1-one; CP, cyclopentanone; 5H2P, 5-hydroxy-2-pentanone; 1,4-PD, 1,4-pentanediol.[1-3,6-14,24]

Heterogeneous, multifunctional catalysts usually offer two or more active sites where each active site plays an independent role in the reaction system. Multifunctional catalysts can play a crucial role in multi-step selective reactions where each active site involves promoting a different step of the reaction. Metal-acid (for hydrogenation and ring arrangement/opening) and bimetal catalysts (for selective hydrogenation steps) are the two multifunctional catalysts of interest in hydrogenation of furfural.[1] Several studies investigated the application of metal-acid catalysts for furfural ring rearrangement. In a study by Zhang et al. 2016, Au metal and TiO_2 as a support was applied for a selective hydrogenation of furfural to cyclopentanone in water at 160 °C and 4 MPa of hydrogen. TiO_2 generated weak Lewis acid sites, promoting the Piancatelli rearrangement, and gold particles are responsible for selective hydrogenation step.[10] Nearly 100% selectivity of cyclopentanone was achieved after 70 minutes of residence time. In another study by Ohyama et al. 2014, Au supported on Nb_2O_5 (source of Lewis acid sites) catalyst was employed to achieve 3-hydroxymethylcyclopentanone (a cyclopentanone derivative) from 5-hydroxymethylfurfural at 140 °C and 8 MPa for residence time of 12 hours.[11] Ohyama et al. 2016 also tested Pt/SiO_2 catalyst in presence of different metal oxides such as Ta_2O_5, ZrO_2, Nb_2O_5, TiO_2, Al_2O_3, SiO_2–Al_2O_3, CeO_2, La_2O_3, and hydrotalcite for synthesizing 3-hydroxymethylcyclopentanone from 5-hydroxymethylfurfural at 140°C and 4 MPa of hydrogen.[12] Metal oxides containing Lewis acid sites resulted in the highest yield of 3-hydroxymethylcyclopentanone and Pt/SiO_2 in presence of Ta_2O_5 catalysts resulted in a yield of 82%. Fang et al. 2015 achieved 86% selectivity of cyclopentanone from furfural hydrogenation using ruthenium supported on MIL-101 (a metal-organic framework with Lewis acid sites) at 160 °C and 4 MPa of hydrogen for 2.5 hours.[13] Cr^{3+} of the MIL-101 support initiated the weak Lewis sites for rearrangement. Weak acid sites in a Ru on mesoporous carbon (CMK-3), combined with an aqueous, acidic environment were recently implicated in the formation of 5-hydroxy-2-pentanone (5H2P) and 1,4-pentanediol from furfural; 5H2P yields as high as 84% were generated in 30h at 60°C; higher temperatures generated 1,4-pentanediol (55%, 100°C, 20h).[6]

The role of bimetallic catalysts for selective hydrogenation of furfural is also important. One advantage of using bimetallic catalysts for furfural hydrogenation is that by providing two different metal active sites, bimetallic catalysts can promote adsorption of hydrogen (through one site) and C=O (through the second site). For example, Fulajtarova et al. 2015 reported that in

hydrogenation of furfural to furfuryl alcohol using a Cu-Pd catalysts, the adsorption of C=O groups on the catalyst is associated with Cu active sites whereas the H atoms are adsorbed on Pd active sites.[14] This mechanism offers an easier interaction between the adsorbed species. In another study by Liu et al. 2016, a selective hydrogenation of furfural to THFA was achieved using Ni-Cu/CNT whereas using Ni only, the catalyst was selective towards furfuryl alcohol only.[15] A Pd-Re/Al_2O_3 catalyst generated higher activity and selectivity for furfuryl alcohol than Pd/Al_2O_3.[16] A Ni-Cu/SBA-15 catalyst enhanced cyclopentanone selectivity and furfural conversion (160 °C,4 MPa) compared to the mono-metal Ni/SBA-15.[17] Rearrangement of the furan ring occurred from furfuryl alcohol. Similarly, a carbon supported Pd-Cu catalyst was selective for hydrogenation of furfural to cyclopentanone in water.[18] Recently, Ni-Co bimetal catalysts on SBA-15 reduced decarbonylation and hydrogenolysis steps to selectively produce tetrahydrofurfuryl alcohol from furfural.[19] Adding Fe to Pd significantly increases furfural turnover frequency in aqueous phase hydrogenations and reduces Pd leaching due to alloying.[20-22,23] More recently, a NiSn bimetal catalyst was shown to produce 1,4-pentanediol (with 5H2P as an intermediate) in high yields (92%, 160°C, 3MPa H_2, 12h) from furfural in an ethanol/water mixture.[24] The NiSn was not only bimetal in nature, but contained acid sites and the material with a balance of weak, medium and strong acid sites generated the highest 1,4-pentanediol yield. The authors proposed that 2-methylfuran undergoes hydrolysis forming 2-hydroxy-2-methyl-tetrahydrofuran with subsequent tautomerism forming 5H2P, which is hydrogenated to 1,4-pentanediol.[24] Overall, bimetal systems increase hydrogenation activity, reduce ring hydrogenation or decarbonylation and hydrogenolysis in the furfural reaction pathway, and stabilize the active metal, relative to mono-metals.

The advantages and challenges of continuous processing renewable platform chemicals, and hydrogenation of furfural have recently been reviewed and assessed.[25-31] However, very few studies have investigated the possibility of continuous 5H2P formation from furfural. Compared to batch operation, continuous production could reduce processing costs and provide a path to scale-up for industrial processes. Continuous furfural hydrogenation has been reported for mono-metals on carbon (e.g., Ni, Cu, Pd, Pt) with a range of solvents (both liquid and vapor phase), with Pd-Cu/silica under vapor phase conditions, a Pd-Fe on mesoporous silica bi-metal, and Pd and Ru on TiO_2 or SiO_2 in the vapor phase with water added.[28-33] The primary products under continuous processing with solvents or vapor phase has been 2-methylfuran (2MF), furfuryl

alcohol (FA), or tetrahydrofurfuryl alcohol (THFA). Interestingly, when water vapor was added to furfural hydrogenation using Ru/TiO_2 or Pd/TiO_2, hydrogenolysis was suppressed (less 2MF) and an enhancement in the rate of cyclopentanone/2-cyclopentenone formation was observed.[33] Au/TiO_2 continuously produced a high yield of cyclopentanone from furfural under aqueous conditions.[10] As mentioned earlier, 5H2P is an important building block and a precursor for 1,4-pentanediol, an important chemical for drug delivery purposes. Furfural can be an inexpensive and green substrate for production of 5H2P. Furfural's commercial unit price is approximately 1/6 of 5H2P. This study focused on comparing bimetal catalysts supported on activated carbon for selective continuous hydrogenation of furfural. Pd-TiO_2, generating weak acid sites, was employed to promote furan ring opening and formation of 5H2P and results were compared to Pd-Fe and Pd-Cu catalysts, providers of strong acid sites.

Experimental Section

Materials and Catalysts. 45 g L^{-1} aqueous furfural (Sigma-Aldrich, 99%) was prepared for each reaction. 0.8% Pd-1.6% Cu and 0.8% Pd-1.6%Fe on activated carbon catalysts were supplied by Applied Catalysts (Laurens, SC) in a monolith form, manufactured by coextrusion of 50% activated carbon and 50% ceramic binder.[34, 38] Each monolith structure was crushed and sieved to a particle size of $0.5 < d_p < 1$ mm. To prepare 0.8% Pd-5% TiO_2 catalyst, a blank activated carbon monolith structure was crushed and sieved into a particle size of $0.5 < d < 1$ mm. In the next step, direct air-hydrolysis method was employed to deposit TiO_2 particles on activated carbon support.[35] Therefore, 2.19 g titanium (IV) isopropoxide (Sigma-Aldrich, 99.999%) was dissolved in 6 mL isopropanol under nitrogen atmosphere. The solution was added to 7 g of crushed activated carbon monolith under stirring condition. The final sample was dried at 120 °C for 2 hours followed by calcination at 300 °C under 100% flow of N_2 (100 ml/min) for 4 hrs. After sample cool down, incipient wetness impregnation method was employed to deposit Pd particles on the catalyst.[36] 0.141 g of Pd(ll) nitrate dihydrate (Sigma-Aldrich, 40% Pd basis) was dissolved in DI water and added to the sample. The sample was dried at 120 °C for 2 hours followed by reduction at 250 °C under 100% flow of H_2 (100 ml/min) for 4 hrs.

Catalyst Characterization. Surface area analysis and pore size analysis were performed as previously described.[34] Micropore analysis was performed using the t-method of de Boer[37] (t is the statistical thickness of an adsorbed film [t (Å) = [13.99/log(Po/P)+0.034]$^{1/2}$]) and the BET surface area data extended to higher pressures (Quantachrome, AUTOSORB-1C; Boynton Beach, Florida). Ammonia-TPD analysis was performed to determine the quantity and strength of acid sites as previously described.[38] FTIR analysis were performed to determine the type of acid sites. The FTIR spectra was obtained using a Thermo Scientific Nicolet 6700 FTIR spectrometer in the wave number range of 4000-399 cm^{-1}. The catalyst samples were diluted in finely powdered KBr. 3 to 4 mg of sample was mixed with 300 to 400 mg of KBr and pressed into a disc in a Hydraulic Press (Carver.Inc; Pressure: 20,000 pounds/ 9 metric tons, Time: 10 min). The disc was placed into the sample holder on the KBr FTIR apparatus. After setting the experimental conditions (resolution:6 ; number of scans : 64) the background was collected for 5-10 minutes to avoid peaks of carbon dioxide and moisture in the spectrum. Prior to KBr dilution, pyridine treatment was performed to determine the type of acid site. The sample was degassed at 150 °C for 2 hours. Next, 50 mg of sample was suspended in 3 mL of 5% pyridine in dry hexane. The mixture was stirred for 1 hour followed by filtering and drying at 100 °C for 1 hour. TPR analysis was performed to determine the reducibility of the catalyst and CO pulse titration was performed to determine the CO uptake of Pd at 40 °C and Pd dispersion.[38] Elemental analysis of fresh and spent catalysts was performed following the Environmental Protection Agency (EPA) ICP method 200.8. Concentrated HNO_3 was added (5 ml) to the sample (~ 0.1g) for microwave digestion following protocols listed in EPA method 3051A. Digested solutions were analyzed by inductively coupled plasma optical emission spectroscopy (ICP-OES, Spectro Arcos FHS16 AMETEK ICP-OES). For Ti analysis, ICP-MS was used, and the samples were digested with hydrofluoric acid.

Analytical. Once the liquid sample was collected from the reactor, it was analyzed in triplicate using gas chromatography with flame ionization detection (GC-FID, HP 5890 Series II) with HP Innowax column (30 m x 0.25 mm x 0.25mm). The GC-FID was operated with the method of inlet temperature 230 °C, detector temperature 240 °C, initial oven temperature of 45 °C for 2.5 minutes followed by a ramp of 10 °C/min for 15.5 minutes and then held at 200 °C for 3 minutes. 1 μL of sample is injected on the GC-FID in triplicate. The concentrations of furfural

(FUR, 99%), furfuryl alcohol (FA, 98%), tetrahydrofurfuryl alcohol (THFA, 98%), 2-methylfuran (2MF, 99%), 2-methyltetrahydrofuran (2MTHF, 99%), cyclopentanol (CPO, 99%), cyclopentanone (CP, 95%), 5-hydroxy-2-pentanone (5H2P, 95%), and 1,4-pentanediol (1,4PD, 99%) were determined using 4-point standard curves (chemicals purchased from Sigma-Aldrich, each point run in triplicate). All standards were prepared in DI water, except for 2MF which was prepared with ethanol as the solvent. The presence of all intermediates and products were confirmed using GC/MS (HP-6890 with HP Innowax column, same method as for GC/FID, 1 μl injection volume, 25:1 split ratio, 0.8 ml/min, 10-500 mass units, MSD ChemStation D.03.00.611 with NIST 2008 database for identification).

Catalytic Reactions. Furfural hydrogenation reactions were performed in a continuous reactor system, designed by Parr Instrument Company, as described previously.[34] 5 g of crushed activated carbon monolith (CACM)[35] was placed between two layers of quartz wool. To determine the optimum conditions for furfural hydrogenation in a continuous reactor system, a series of experiments at temperatures ranging from 120 to 180 °C (LHSV of 1.32 h^{-1}, 300 psig or 2.1 MPa), pressures of atmospheric to 300 psi (0.1-2.1 MPa, LHSV of 1.32 h^{-1}, 180°C), and liquid flow rates of 0.5 to 6 mL/min (various LHSV at 180°C and 300 psig) were performed using Pd-TiO_2 on crushed activated carbon monolith (Pd-TiO_2/CACM), Pd-Cu on crushed activated carbon monolith (Pd-Cu/CACM), and Pd-Fe on crushed activated carbon monolith (Pd-Fe/CACM).

Turnover frequency (TOF, h^{-1}) was calculated as,

$$TOF = \frac{[F_{FUR,in} - F_{FUR,out}]}{W_{cat} L_{Pd} D} MW_{Pd} \quad (1)$$

Where F_{FUR} is the molar rate in and out of the reactor (moles/h), W_{cat} the mass of catalyst (g), L the Pd loading as wt%, D the dispersion of Pd as measured by CO pulse titration (moles Pd adsorbing CO/total moles of Pd), and MW_{Pd} the molecular weight of Pd (TOF as moles furfural reacted or mole of product formed/mole of active Pd/h or h^{-1}). TOF for products was calculated as $F_{product}$ (moles/h)* $MW_{Pd}/[W_{cat}*L_{Pd}*D]$. Additional kinetic parameters were calculated as described in the supporting information.

Carbon closures for changing LHSV were 82 ± 7%, 67 ± 1.5%, and 65 ± 8% (180°C, 300 psig) for Pd-Ti/CACM, Pd-Cu/CACM, and Pd-Fe/CACM respectively. For Pd-Ti/CACM carbon closures were consistent with temperatures from 120 to 180 °C (82 ± 5%, LHSV 1.32 h^{-1}, 300 psig). For Pd-Cu/CACM, carbon closure was higher at lower reaction temperatures; e.g., carbon closure ranged from 84-88% from 120 to 160°C, but declined to 65% at 180°C (LHSV 1.32 h^{-1}, 300 psig). The trend was different for Pd-Fe/CACM; carbon closures were low at all temperatures (58 ± 10.5, LHSV 1.32 h^{-1}, 300 psig). When studying the effect of pressure (LHSV 1.32 h^{-1}, 180°C) carbon closure increased with pressure for Pd-Ti/CACM (30% at 14.7 psig to 88% at 300 psig). For Pd-Cu/CACM and Pd-Fe/CACM carbon closure increased with pressure, but not to the same extent as Pd-Ti/CACM (33-49% at 14.7 psig to 55-65% at 300 psig – see Figure SI-7 for the plots). Overall, Pd-Ti/CACM had higher carbon closures compared to Pd-Cu and Pd-Fe/CACM indicating the formation of side products that were not captured in our analysis for these catalysts. The reduction in carbon closure for Pd-Cu/CACM at 180°C relative to the lower temperatures also suggests the promotion of a side reaction not anticipated in our analysis (Figure SI-7).

Results and Discussion

Catalyst Characterization. NH_3-TPD results showed medium acid site peaks between 300-500 °C for all three catalysts. Using probe molecules and TPD acid site strengths have been defined as weak (150-300°C), medium (300-500°C), and strong (>500°C).[39] As previously reported, the presence of the medium acid sites is attributed to metal oxides such as silica and alumina in the monolith structure.[38] In addition, Pd-TiO_2/CACM demonstrated weak acid sites at approximately 150 °C, whereas Pd-Fe/CACM results indicated strong acid sites at 525 °C (**Figure 2 and Table 1**). To determine the type of acid sites, FTIR spectra was recorded for each catalyst. The FTIR spectra of CACM support (**Figure SI-1**) shows a band around 1385 cm^{-1}, associated with -COOH in activated carbon support.[40] The bands around 1530, 1550 and 1640 cm^{-1} are associated with pyridine adsorption at Bronsted acid sites, attributed to the presence of metal oxides in the CACM binder.[40-42] Pd-Cu/CACM, Pd-Fe/CACM and Pd-TiO_2/CACM FTIR spectra **(Figures 3-5)** showed additional bands around 1618 cm^{-1}, associated with Lewis acid sites, and 1480 cm^{-1}, associated with both Lewis and Bronsted acid sites.[12, 43] All three catalysts indicated both

Bronsted and Lewis acid sites. **Figure 6** shows SEM-EDS images of Pd-TiO_2/CACM (SEM-EDS images of the mono-metal and other two bi-metal catalysts have been previously reported – **Figures SI-R1, R2, R3 for review only**).[38,44] Most of the Pd particles are located very close to TiO_2 particles. Due to high reactivity of titanium (IV) isopropoxide, employed for Pd-TiO_2/CACM synthesis, with moisture in the air, at some regions TiO_2 particles were formed quickly, resulting in large TiO_2 particles. Therefore, at some regions on Pd-TiO_2/CACM catalyst the density of TiO_2 particles is high.

Figure 7 indicates TPR analysis of the three catalysts. Since our catalysts were reduced at 250°C in flowing 100% H_2 before use, one can suggest PdO is completely reduced to Pd^o in all catalysts when analyzing the TPR results relative to the literature (Fig.7). As noted by others and in our past work using Pd/ACM[38] and for Pd/TiO_2/ACM, the low temperature negative peaks are indicative of weak interaction of PdO with carbon (Fig. 7).[45] The two positive peaks in the Pd/TiO_2/CACM after the negative peaks (180°C, 220°C) indicate interaction with the support, possibly TiO_2 and the ceramic binder. These temperatures are slightly lower than in previously reported Pd/ACM (205°C, 287°C), but significantly higher than Pd/GAC (125°C).[38] Figure 7 also suggests the presence Pd-Cu and Pd-Fe, since others report alloying at 200-220°C for Pd-Cu/carbon and 240°C in Pd-Fe/carbon.[46,47] Pd-Cu/CACM indicated peaks at 220 and 320 °C and Pd-Fe/CACM demonstrated two peaks at 250 and 400 °C. However, since complete reduction did not occur (~320°C for Pd-Cu and 400°C for Pd-Fe, Fig.7), copper and iron oxide forms are probably also present in the bimetals. Pd-TiO_2/CACM showed one small negative, one positive and one sharp negative peak at 42, 44 and 63 °C, respectively. The negative peaks are attributed to decomposition of palladium hydride (β-PdH), formed during the positive peak at 44 °C or initial purge of hydrogen during TPR, due to the presence of freely available PdO on the surface of the catalyst.[45] This effect has been associated with presence of large Pd particles since small Pd particles usually have stronger interaction with the catalyst support and do not react with hydrogen in low temperatures.[49] The lack of negative peaks in Pd-Cu/CACM and Pd-Fe/CACM TPR can indicate an interaction between Pd and the second metal

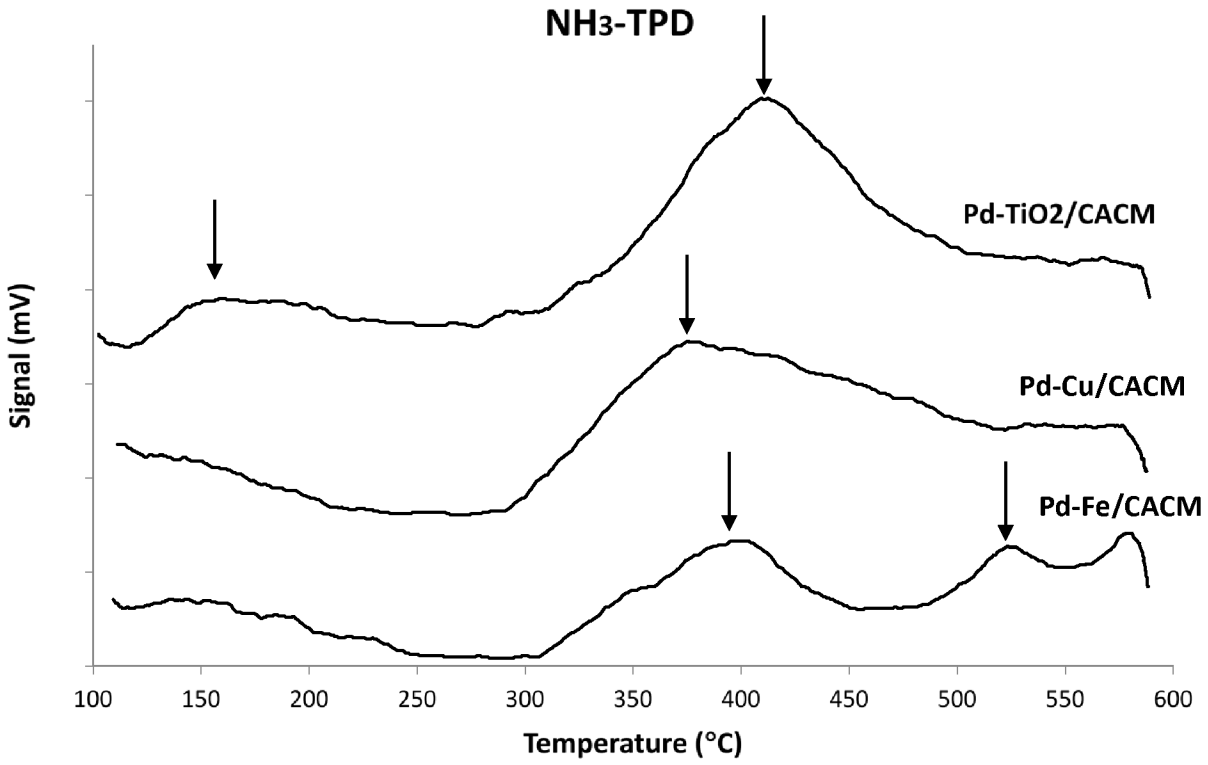

Figure 2. Ammonia TPD analysis of bi-metal carbon catalysts pre-reduced with H_2 (100% H_2, 2 h, 250 °C).

Table 1: Physical properties of the catalysts

Catalysts Properties	Pd-TiO_2/CACM	Pd-Cu/CACM	Pd-Fe/CACM
Metal Loading (wt.%)[a]	0.8 Pd-4.14 TiO_2	0.65 Pd-1.7 Cu	0.50 Pd-1.71 Fe
Surface Area (m^2/g)	736	562	627
Pore Volume (cm^3/g)	0.63	0.50	0.54
Average Pore Size (radius, Å)	34.2	35.9	34.8
Micro-Pore Volume[b], (cm^3/g)	0.022	0.009	0.024
Acid Sites at 150 °C, (μmoles NH_3/g)	50	0	0
Acid Sites at 400 °C, (μmoles NH_3/g)	94	231	53
Acid Sites at 525 °C, (μmoles NH_3/g)	0	0	38
CO uptake[c] (μmoles CO/g)	0.46	0.41	0.63

[a], Calculated from elemental analysis/ICP-MS
[b], Estimated from t-plot analysis
[c], CO uptake from CO pulse titration at 40 °C
CACM is crushed activated carbon monolith

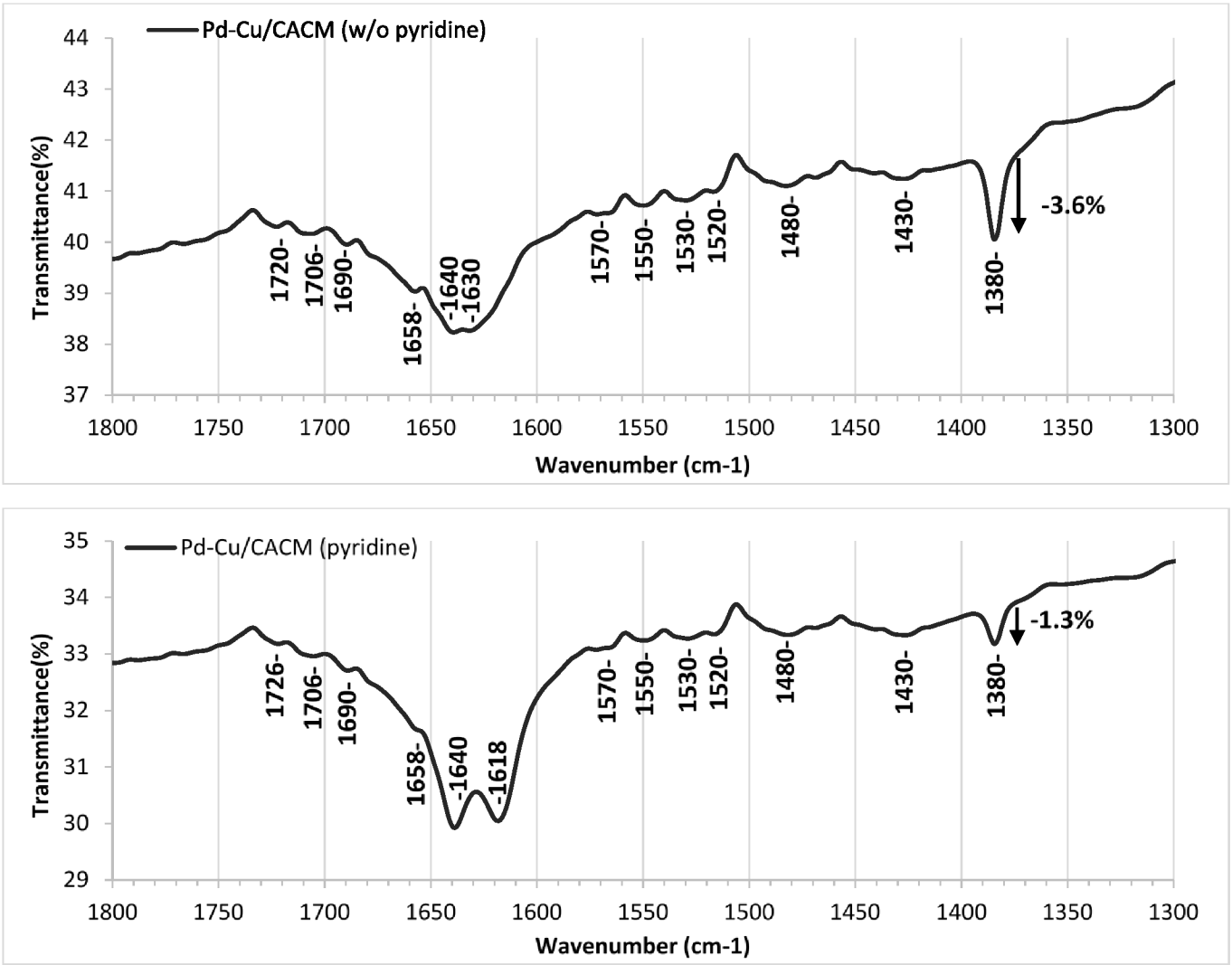

Figure 3. FTIR analysis of Pd-Cu/CACM.

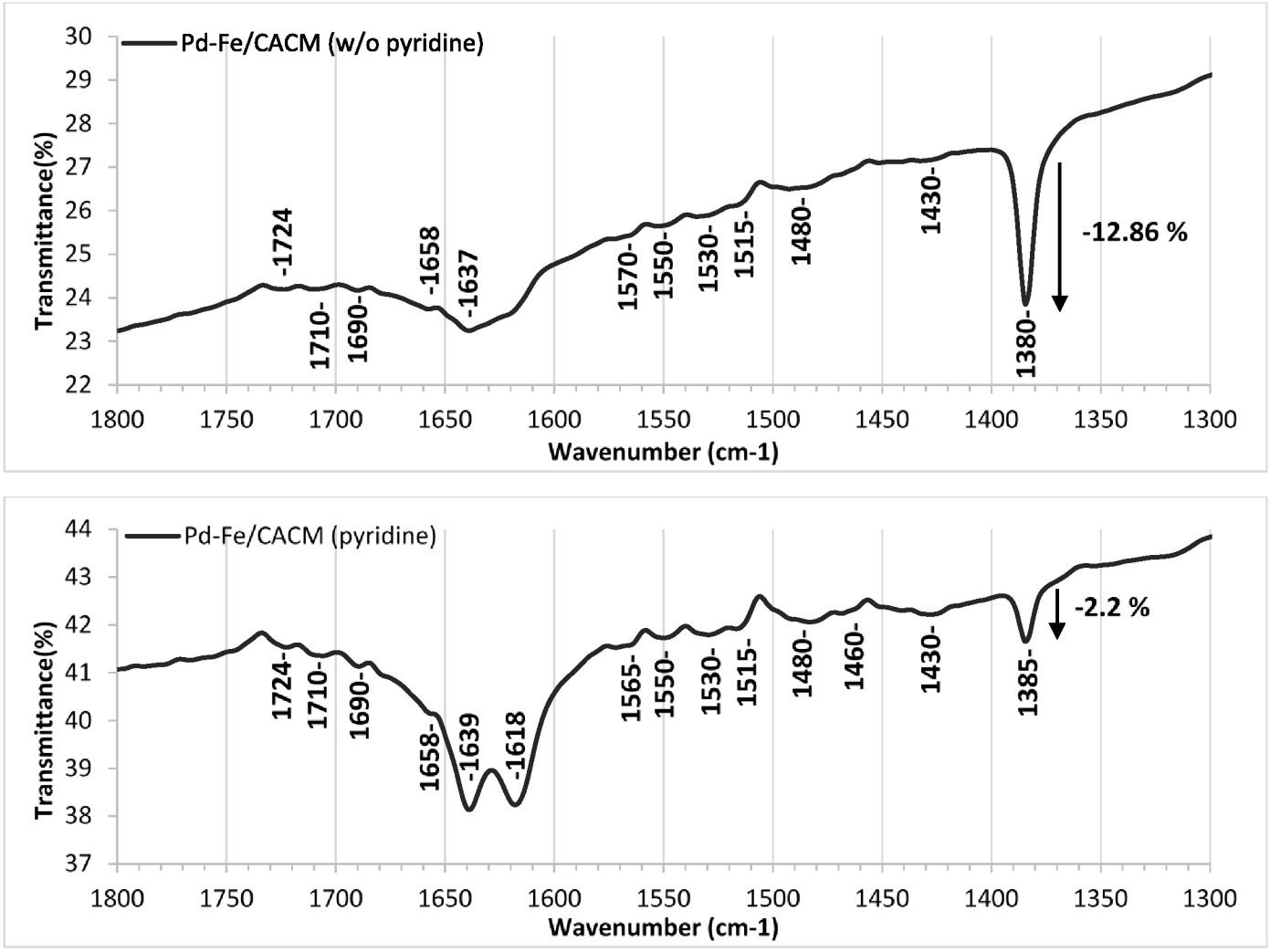

Figure 4. FTIR analysis of Pd-Fe/CACM.

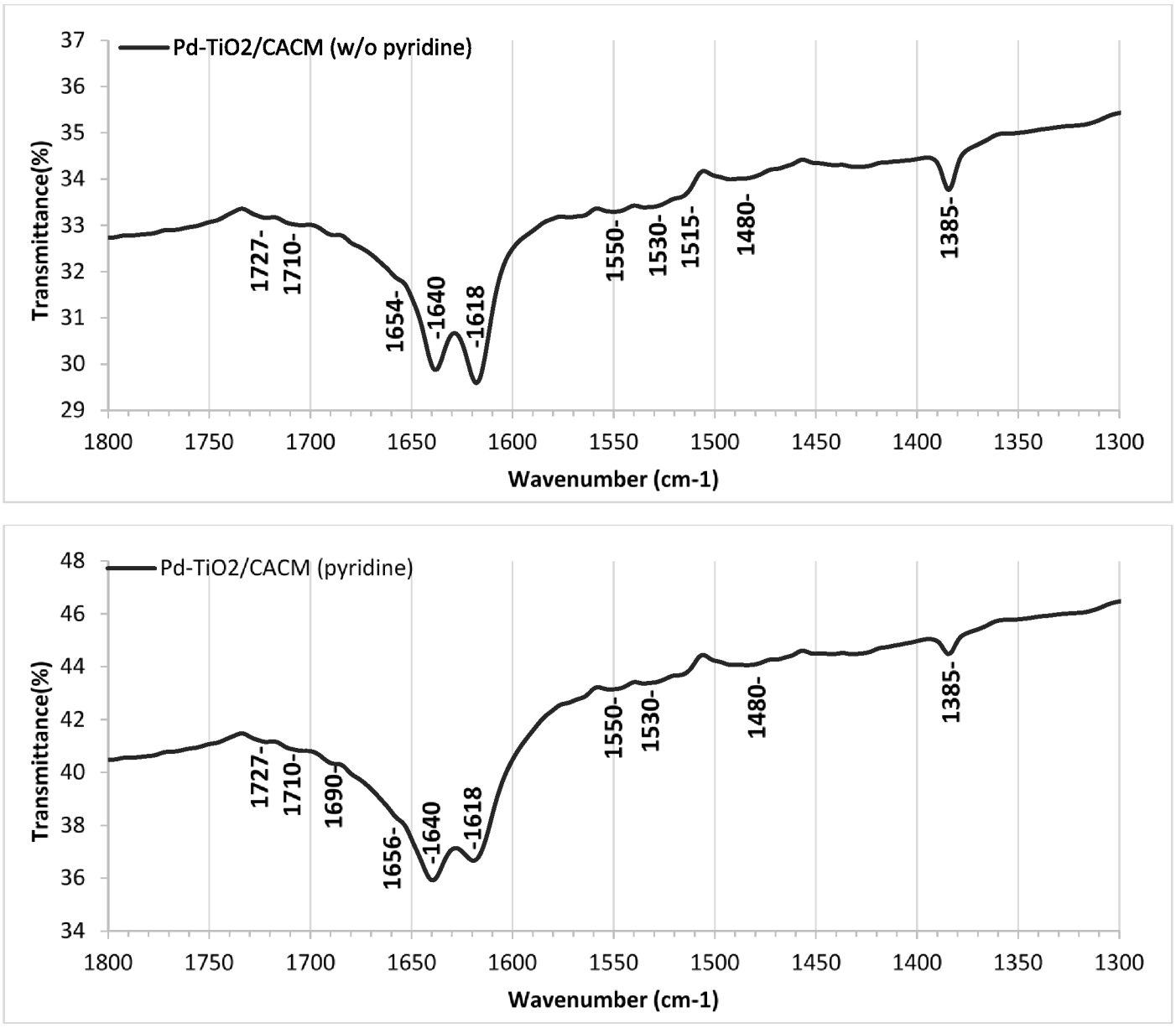

Figure 5. FTIR analysis of Pd-TiO_2/CACM

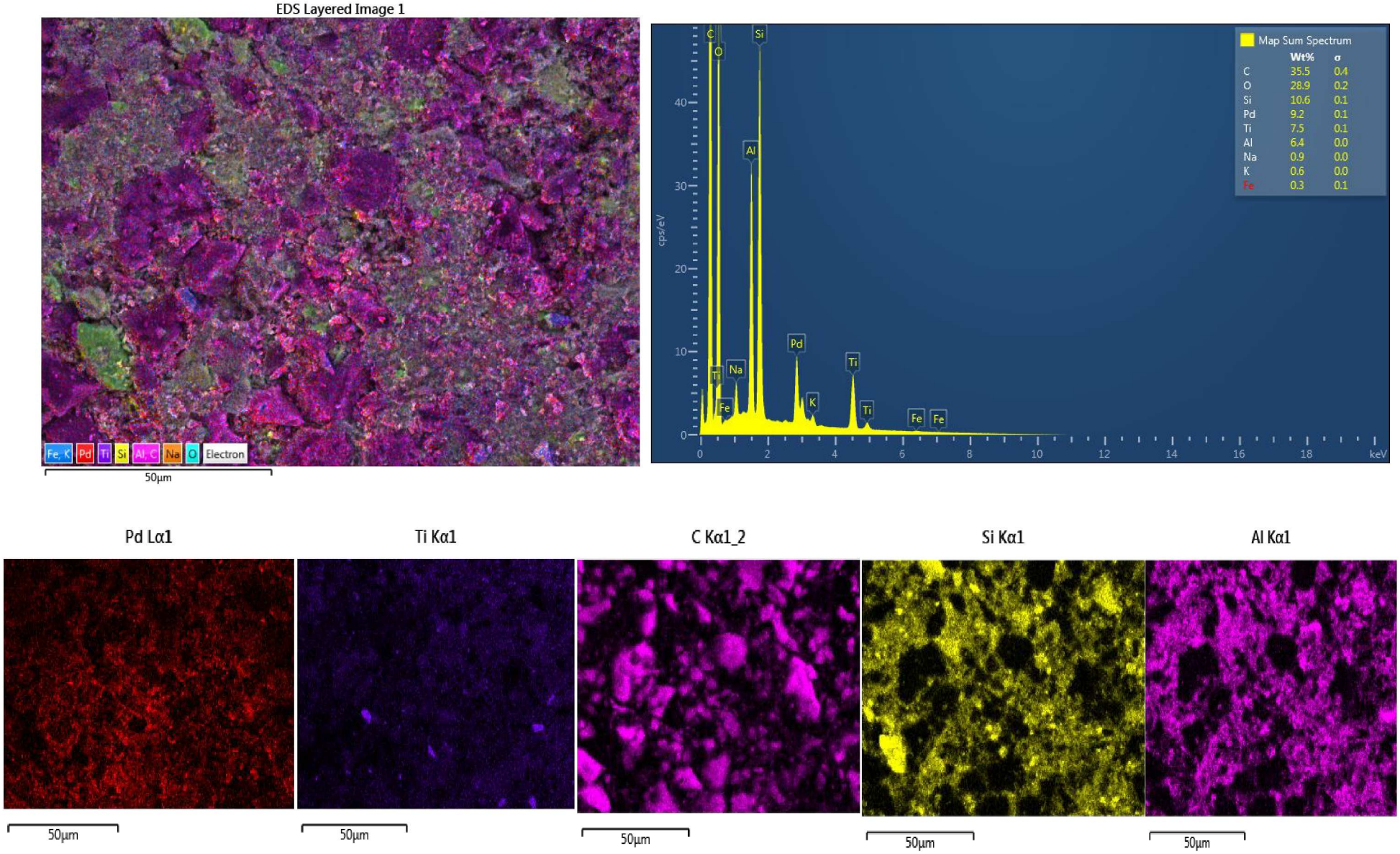

Figure 6. SEM-EDS images of Pd-TiO_2/CACM.

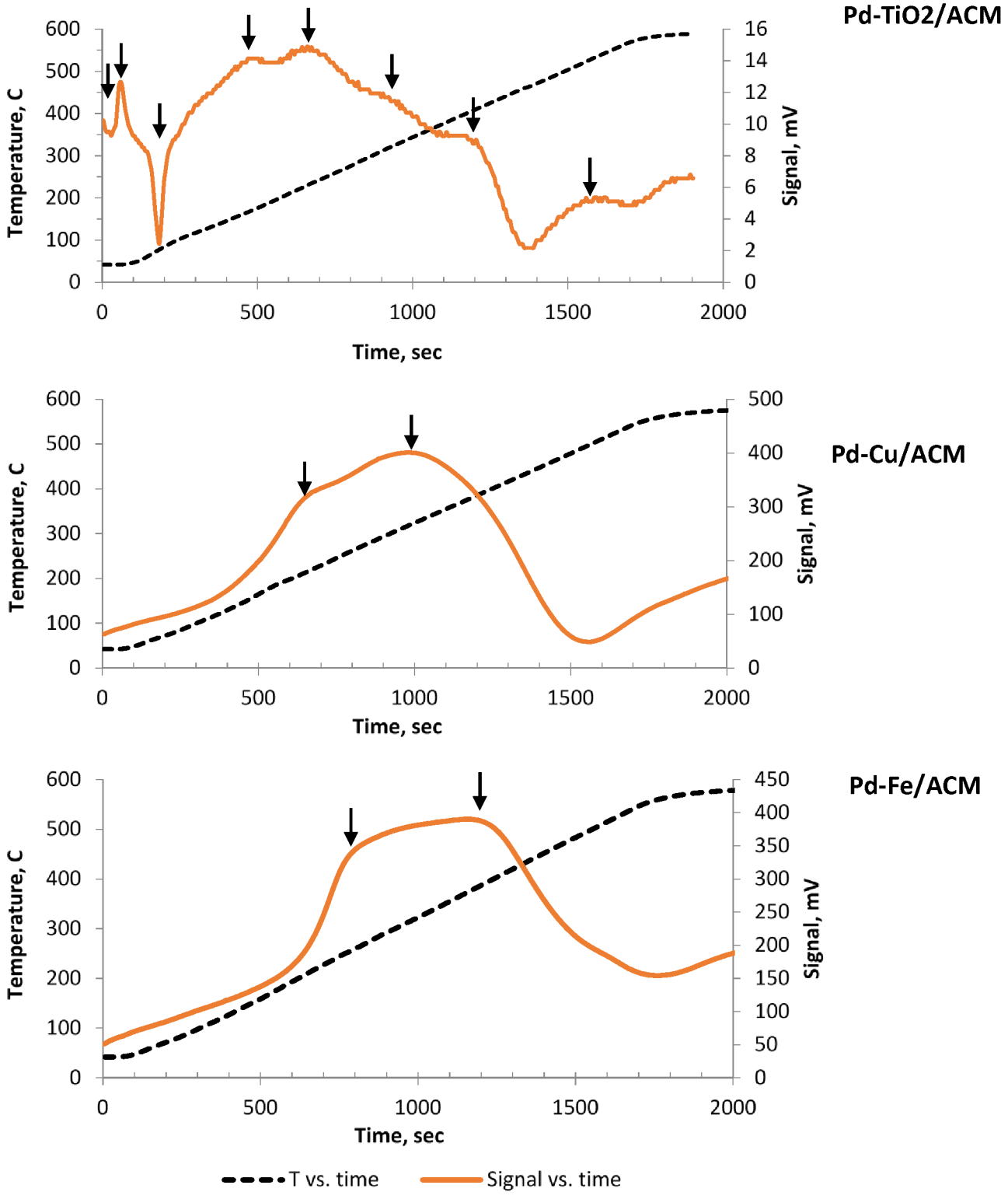

Figure 7. Temperature programmed hydrogen reduction of activated carbon catalysts.

which prevents the larger Pd particles from reacting with hydrogen at low temperature. Pd-TiO_2/CACM showed 5 additional peaks at 180, 220, 315, 422 and 525 ° C. The peaks at 180 and 220 °C have been associated with the reduction of Pd^{2+} to Pd on carbon.[49] The peaks at 220 °C, 315 °C and 422 °C could also represent the reduction of Pd on TiO_2 [48,50-52] or the binder component such as silica or alumina.[53] These peaks at 220 °C and 315 °C may be associated with partial reduction of TiO_2 particles as it has been reported that the presence of Pd° can lower the reduction temperature of TiO_2 due to the role of Pd° in providing dissociated hydrogen for TiO_2 through hydrogen spillover effect.[48,50-52] The temperatures for these peaks were lower than in Pd/ACM (205°C, 287°C vs. 180°C, 220°C), but significantly higher than Pd/GAC (125°C).[38] Titania (Ti^{4+}) is reportedly reduced to Ti^{3+} in the presence of Pd at 200°C, due to hydrogen spillover.[50-52] We have measured hydrogen spillover via H_2 pulse titration in our past work with the Pd/ACM catalyst.[54] TiO_2 without Pd reportedly has two reduction peaks in H_2-TPR, one at 275°C and 400°C.[52] Upon Pd addition to TiO_2 the first peak is lowered to 220°C and the second generates shoulders at 350°C and 400°C.[52] Electrochemically deposited or wet impregnated Pd on TiO_2 indicates a significant reduction in peak temperature as well to 200°C and 350°C.[51] These results suggest the peak at 220°C is indicative of Ti^{4+} reduction to $Ti^{3+}$and the higher peaks at 315°C and 422°C account for complete reduction (Fig. 7). The peak at 525 °C is due to decomposition of oxygen functional group from activated carbon that can occur at temperatures >300°C.[55]

We also performed XRD on the ACM catalysts. Due to incomplete metal oxide reduction, low metal loading (Pd, Cu, Fe), and high dispersion (Pd), XRD analysis of the Pd-Cu, Pd-Fe, Pd-Ti/CACM did not indicate Pd, Cu, Fe, TiO_2 or oxide structures (Fig. SI-2). The ACM alone had peaks indicative of graphite (21 °, 26 ° 2θ)[56] and other peaks (28°, 35°, 36.5°, 39.5°, 40.5°, 41.6°, 42.9°, 46°, 50°, 60°, 68° 2θ), which were present in all materials, probably due to the ceramic binder. Anatase on carbon reportedly has peaks at 25.3°, 37.8°, 48°, 53.9°, 55°, 62.7°, 68.8°, 70.3° 2θ and rutile a peak at 27.5° 2θ.[57] These results suggest crystalline TiO_2 was either not formed or dispersion was high in the Pd/TiO_2/CACM and for the Pd-Ti, Pd-Cu and Pd-Fe catalysts, Pd loadings were low and dispersions high. This effect has been noted on other bimetal carbon catalysts at low metal loading (~1%) and TiO_2 on silica.[58,59]

Surface area analysis of the three catalysts indicated a slightly higher pore volume and surface area for Pd-TiO_2/CACM (**Figure SI-3 and Table 1**). Pd dispersion was similar between the Pd-TiO_2 and Pd-Cu catalysts and dispersion was higher in Pd-Fe (Table 1). Except for acid site strength and concentration, and Pd interaction with the second metal or metal oxide, the surface properties of the three catalytic materials were not significantly different.

Effect of Temperature and Pressure. A series of reaction temperatures ranging from 120 to 180 °C (at 1.32 1/h LHSV, 300 psig) were tested to determine the effect of this parameter on selectivity and space time yield of products (**Figure SI-4, SI-5)**. In presence of all three catalysts, FA selectivity decreased over the range of tested temperatures. THFA selectivity increased to a maximum of 37% for Pd-TiO_2/CACM, 44% for Pd-Fe/CACM and 59% for Pd-Cu/CACM at temperature of 140 °C then decreased with increasing temperature. In presence of all three catalysts, the highest selectivity of 2MF was achieved at 180 °C, with Pd-TiO_2/CACM achieving the highest 2MF selectivity of 38%. Pd-TiO_2/CACM also achieved the highest 2MTHF and CP selectivity although less than 5% of these two products were determined for all catalysts over the range of tested temperatures. The highest selectivity of 17% was achieved for 5H2P, a ring opening product of furan ring, at 140 °C in presence of Pd-TiO_2/CACM.

A second series of reactions were performed to determine the effect of pressure, ranging from atm to 300 psig at 1.32 1/h LHSV and 180 °C, on selectivity and space time yield of products **(Figure SI-6, SI-7)**. The highest FA selectivity in presence of all three catalysts was determined at atmospheric pressure. Comparing the FA selectivity of the three catalyst at atmospheric pressure, Pd-Cu/CACM achieved the highest selectivity of 38% whereas Pd-TiO_2/CACM and Pd-Fe/CACM resulted in 11% and 14% FA selectivity, respectively. At pressures higher than atmospheric pressure, less than 5% of FA selectivity was determined for all the catalysts. Pd-Cu/CACM also achieved the highest THFA selectivity of 37% at 200 psig. In presence of Pd-Fe/CACM, THFA selectivity reached a maximum of 24 % at 100 psig and did not change significantly with increasing pressure. The highest selectivity of THFA in presence of Pd-TiO_2/CACM was 24%, achieved at 300 psig. 2MF selectivity increased with increasing pressures. At 300 psig, the 2MF selectivity of 38%, 25% and 16% for Pd-TiO_2/CACM, Pd-Cu/CACM and Pd-Fe/CACM were achieved, respectively. Except at 100 psig in presence of Pd-Fe/CACM where a 2MTHF selectivity of 14% was achieved, at all tested pressures less than

10% of 2MTHF and CP selectivity was determined. At 200 psig, 5H2P selectivity reached a maximum of 24%, 23% and 16% in presence of Pd-Fe/CACM, Pd-Cu/CACM and Pd-TiO_2, respectively and then decreased with increasing pressure to 300 psig. Overall, 5H2P selectivity and STY increased with temperature and pressure, and carbon closures were higher at P≥200psig (Figure SI-8), thus a reaction temperature and pressure of 180°C and 300 psig was used for further studies.

Effect of Liquid Residence Time. Next, the effect of liquid flow rate on furfural conversion, product selectivity, space time yield, and turnover frequency was determined (**Figures 8-9;** 0.5 to 6 mL/min, LHSVs 1.32 to 15.8 1/h, 180 °C, 300 psig). High furfural conversions (90% or higher) were achieved for all three catalysts at LHSVs of 1.32, 3.96 and 7.92 1/h. At 15.8 1/h, conversions of 86%, 85% and 76% were achieved for Pd-Cu/CACM, Pd-TiO_2/CACM and Pd-Fe/CACM, respectively. In presence of all three catalysts, FA selectivity decreased with increasing residence time or decreasing LHSV. The highest FA selectivity of 42%, 32% and 30% for Pd-Cu/CACM, Pd-Fe/CACM and Pd-TiO_2/CACM occurred at 15.8 1/h LHSV, the shortest residence time. A high FA space time yield of 260 g/Lcat/h was achieved in presence of Pd-Cu/CACM. THFA selectivity decreased with decreasing residence time. At LHSVs of 3.96 and 7.92 1/h, Pd-Fe/CACM demonstrated a significantly higher selectivity towards THFA compared to the other two catalysts. At all residence times, Pd-TiO_2/CACM achieved the highest 2MF selectivity of 38% at the longest residence time among all three catalysts. In general, 2MF selectivity increased with increasing residence time. Very low selectivity of 2MTHF (less than 5%) was determined using Pd-TiO_2/CACM and Pd-Cu/CACM. Using Pd-Fe/CACM the 2MTHF selectivity increased to 11% at LHSV of 3.96 1/h then decreased with increasing LHSV. Less than 4% of CP selectivity was determined in presence of all three catalysts. Among the three catalysts, the highest 5H2P selectivity was achieved in presence of Pd-TiO_2/CACM at LHSVs of 3.96, 7.92 and 15.8 1/h. At 7.92 1/h, 39% 5H2P selectivity and 134 g/Lcat/h STY was achieved in presence of Pd-TiO_2/CACM whereas at the same LHSV the other two catalysts demonstrated approximately 11% selectivity and 43 g/Lcat/h yield **(Figure 9)**. When calculating turnover frequency (based on catalyst Pd loadings and CO pulse titration), trends similar to STY were observed. The most noticeable differences were the much larger 2MF and 5H2P TOF's using Pd-TiO_2 (116 h^{-1} 2MF, 190 h^{-1} 5H2P) and much higher FA TOF (557 h^{-1}) using Pd-Cu compared to the other catalysts (**Figure SI-8**).

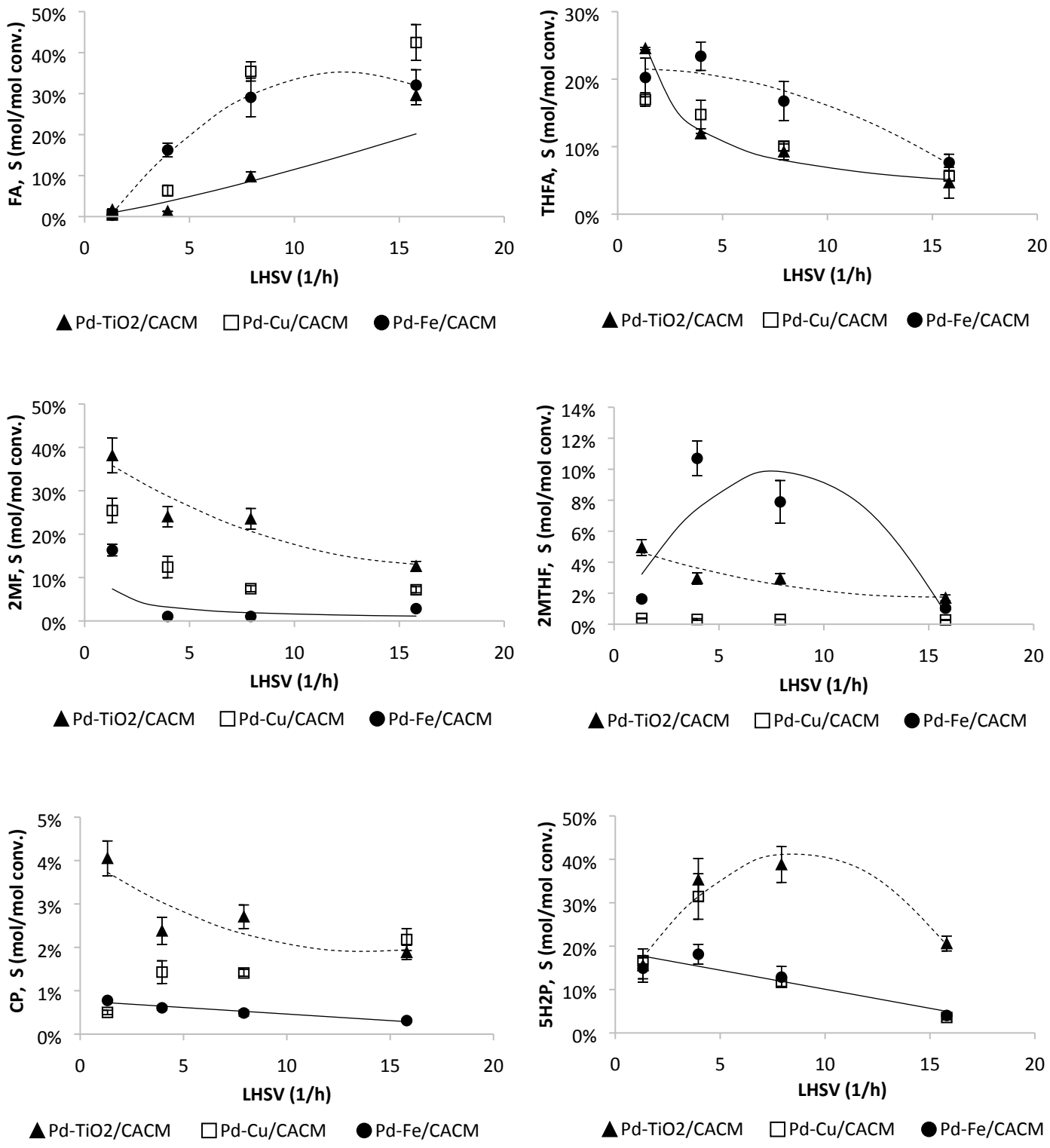

Figure 8: Effect of liquid hourly space velocity (LHSV) on product selectivity. P = 300 psig, T = 180 °C, 5 g of catalyst.

Structure/Function Analysis. NH_3-TPD results indicated the presence of both weak (150 °C peak) and medium (400 °C peak) acid sites for Pd-TiO_2/CACM, whereas the other two catalysts demonstrated only medium to strong acid sites **(Figure 2 and Table 1)**. All three catalysts indicated the presence of both Lewis and Bronsted acid sites. As indicated in previous work using Pd-Cu and Pd-Fe supported on activated carbon monolith structures for aqueous furfural hydrogenation, adding Fe and Cu to Pd shifted selectivity from 2MF to FA and THFA possibly due to adsorption of C=O at Fe and Cu sites. [44 (In Review)] Therefore, it was expected to see a similar selectivity effect using the crushed form of the bimetal monolith catalysts. Incorporating TiO_2 in Pd catalyst demonstrated the highest 5H2P selectivity and TOF at the two shortest residence times among the three catalysts (Table 2, Fig. SI-9). Higher 5H2P selectivity and TOF in the presence of TiO_2 can be attributed to weak acid sites at 150 °C, demonstrated by NH_3-TPD results. Since TiO_2 is known to only generate Lewis acid sites under most conditions,[60] and only Bronsted acid sites were observed in ACM only, we suggest that the weak acid sites were of the Lewis acid nature in Pd/TiO_2/CACM. The reduced medium acid site concentration and lack of strong acid sites in Pd/TiO_2 may have also contributed to the higher carbon closure since medium to strong acid sites in an aqueous environment can catalyze furfural oligomerization. The weak acid sites can promote furan ring opening and further hydrogenation steps result in formation of 5H2P. Liu et al. 2015 also reported that presence of weak acid sites in Ni-bearing hierarchical Y zeolites promoted the furfural ring rearrangement whereas zeolites with medium-strong acid sites demonstrated lower yield of ring rearrangement product with higher furfural conversion.[61] Zhang et al. 2016 reported a high yield of furfural rearrangement ring product in presence of TiO_2, known to provide weak Lewis acid sites.[10] It has been reported that the presence of silica as a catalyst support for Ir–ReO*x* and a source of acid sites, resulted in formation 1,4-pentanediol, a hydrogenation product of 5H2P.[62] Weak acid sites in a Ru on mesoporous carbon (CMK-3) were implicated in the formation of 5-hydroxy-2-pentanone (5H2P).[6] The weak acid sites were in the same range as we report (100-200°C, NH_3-TPD) and partially reduced Ru on CMK resulted in a Ru^+ species implicated as the weak acid site. Carbon dioxide was also charged in this system and it was suggested the acidic environment combined with the weak acid and metal sites catalyzed the formation of 5H2P (73%, 60°C, 30h) and 1,4-pentanediol at higher temperatures (90%, 80°C, 20 h). Recently, this group has used a combination of Ru/FeOx/Activated Carbon (AC) with a

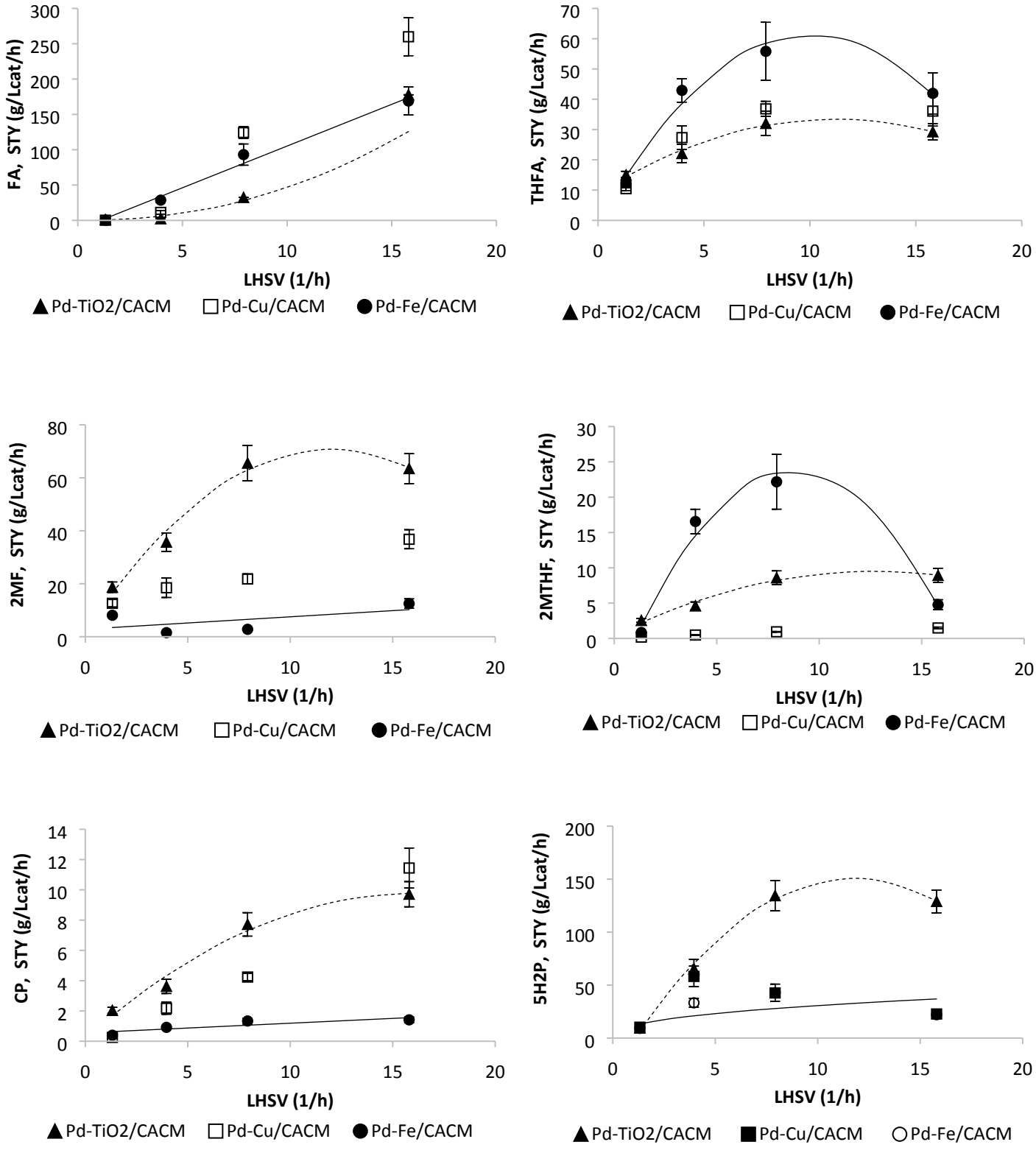

Figure 9: Effect of LHSV on product STY. P = 300 psig, T = 180 °C, 5 g of catalyst.

strong acid resin (Amberlyst 15) to hydrogenate furfural to 5H2P and 1,4-pentanediol.[63] The Fe promoted Ru on AC catalyst had higher Ru dispersion and a lower level of acid sites, compared to Ru/AC. The lower level of acid sites and weak acid sites (150°C, NH_3 TPD) in the Ru/FeOx/AC reduced hydrolysis of furfuryl alcohol (generated by Ru hydrogenation of furfural) to levulinic acid and promoted 5H2P formation from the ring opened product initiated by the strong acid sites in the resin. An imbalance between acid and metal sites promoted 5H2P formation, whereas balanced acid and metal sites produced primarily 1,4-pentanediol.[63] Given the rapid formation of furfuryl alcohol (FA) and subsequent formation of 5-hydroxy-2-pentanone (5H2P) and low levels of cyclopentanone (CP), we suggest FA is stabilized by the Lewis acid sites and undergoes protonation (H^+), and dehydration/hydration/rearrangement steps to form a pentadienyl cation intermediate, which is subsequently hydrogenated via dissociated H_2 on Pd sites to 5H2P.[3,6] A speculative reaction pathway based on our results and the literature is noted in Figure SI-10.[3,6] We note the possibility that Bronsted acid groups are formed on TiO_2, since it has been reported that at high water density H_2O dissociates on TiO_2 to form OH^- and H^+.[60] Piancatelli rearrangement of FA and subsequent dehydration and hydrogenation of 4-hydroxy-2-cyclopentenone generates the low levels of cyclopentanone (Fig.1).

We also note that the Pd/TiO_2 catalyst did have higher 2MF selectivity, STY, and TOF compared to the other catalysts (**Figures 8-9, SI-8**). In past work using the same base material as used in this work, a Pd on activated carbon monolith gave similar 2MF selectivity from furfural over the same LHSV range, yet very low 5H2P selectivity.[38] It is speculated that a fraction of the Pd remained segregated from Ti and the weak acid sites, thus catalyzing the hydrogenation/dehydration steps to 2MF (**Figure 1**). This concept is partially supported by the SEM-EDS and H_2-TPR results indicating isolated Ti aggregates and separate low temperature reduction steps for PdO in the Pd/TiO_2 catalyst (**Figure 7**). Better interaction between Pd and Ti could further improve 5H2P selectivity and STY and potentially promote hydrogenation of 5H2P to 1,4-pentanediol (1,4PD). Low levels of 1,4PD were observed at the lowest LHSV (1.32 1/h) using Pd/TiO_2 catalyst (0.1 g/L) compared to higher levels using Pd-Cu (3 g/L) and Pd-Fe (0.6 g/L) in which there was better interaction between Pd and the second metal.

Continuous Furfural Hydrogenation: Benchmark space time yield or conversions for continuous processes have been published by industry and in patents. Shell Global Solutions developed 1%Pt/TiO_2 catalysts and demonstrated continuous hydrogenation of levulinic acid to γ-valerolactone (gVL) at space time yields of 10,000 g/kg-cat/h and STY's for hydrogenation of gVL to valeric acid of 2,000 g/kg-cat/h using 0.7%Pt/HZSM-5/SiO_2.[64] Aqueous phase hydrogenation of maleic acid to THF using a Ru-Re on carbon catalyst generated a STY of 600-1,200 g THF/kg-cat/h.[65] As noted in Fig. 9, our STY's for 5H2P (134 g/Lcat/h or 610 g/kg-cat/h) approach these values indicating possible industrial viability.

Comparison of mono-metal, bi-metal, and bifunctional catalysts in continuous furfural hydrogenation indicates notable differences (Table 2). In comparing PdTiO_2/CACM, Pd-Cu/CACM, and Pd-Fe/CACM within this group and the literature we used results from the initial testing of W/F and time on streams limited to 110, 122, and 127 min for Pd-Cu, Pd-Fe, and Pd-Ti, respectively. In calculating TOF we assumed no loss of Pd and used Pd dispersions and loadings for the fresh catalyst. When comparing with the literature we used directly published turnover frequency (TOF) and selectivity data or used equation 1 and the reported metal dispersion to calculate TOF. Comparison was limited to continuous processing since our primary goal was to determine the feasibility of continuous operation. Mono-metal systems had lower TOF and produced little Piancatelli rearrangement products (e.g., cyclopentanone; entry A-C, E). The bi-metal systems significantly increased furfural TOF (compare C&D, and E with F&G) . Adding weak acid sites and creating a metal-acid catalyst (Pd/TiO_2/CACM) significantly increased 5H2P selectivity and TOF, without significantly reducing furfural hydrogenation activity (entry H). An Fe promoted Ru on activated carbon catalyst in the presence of Amberlyst-15 primarily produced 1,4-pentanediol (via hydrogenation of an 5H2P intermediate; entry I). The TOF for this system was low (probably due to the low flow rate and temperature). Pd and Au on TiO_2 both produced high yields of cyclopentanone (entry J) and the Au/TiO_2 generated a 1,4-pentanediol STY of 848 g/kg-cat/h (estimated from continuous PBR data, entry K). It is unclear as to why the Pd/TiO_2/CACM primarily produced 5H2P, yet the Pd/TiO_2 and Au/TiO_2 produced cyclopentanone. The different synthesis methods and supports (activated carbon vs. TiO_2) may have created different active site environments stabilizing different intermediates from furfuryl alcohol ring opening.

Table 2 - Comparison of furfural turnover frequency (TOF, h^{-1}) and selectivity (%) for various catalysts in continuous furfural hydrogenation reactions.

Entry	*Catalyst*	*Reactant/ Solvent*	*T(°C)*	*P (bar)*	*X (%)*	*TOS[a], min*	*TOF,h^{-1} (FUR)*	*FA*	*THFA*	*2MF*	*5H2P/ 14PD*	*CP*	*Reference*
A	3% Pd/AC	FUR/CPME	150	50	97	12-48 (31.2)[b]	55	25	56	5	-	0	28
B	4.93%Pd/PowderC	FUR/EtOAc	90	50	77	20 (34)[b]	24	-	-	High	-	-	**29**
C	0.5%Pd/Silica	Furfural vapor	150	20	2.5	120-240 (1.7)[b]	344	47	44	-	-	-	30
D	0.4%Pd-9%Cu/Silica	Furfural vapor	150	20	12.0	120-240 (1.7)[b]	579	85	5	10	-	-	30
E	**1.2% Pd/ACM**	FUR/water	180	20	46	20 (22)[b]	248	21 (52.5)[c]	2	18 (43.5)[c]	0	0	**38**
F	**0.5% Pd-1.7%Cu/cACM**	FUR/water	180	20	86	110 (19)[b]	1138	43 (483)[c]	6	7	4 (41)[c]	2	**This work**
G	**0.65%Pd-1.7%Fe/cACM**	FUR/water	180	20	74	122 (19)[b]	838	32 (269)[c]	6	3	5 (34)[c]	0	**This work**
H	**0.8%Pd-4%TiO_2/cACM**	FUR/water	180	20	84	127 (19)[b]	798	30 (236)[c]	5	11	21 (165)[c]	1.6	**This work**
I	1.5%Ru/6.3%FeOx/AC+Amb15	FUR/water	80	2	100	10,500(13,500)[b]	1.04	-	-	-	78 (0.88)[c,d]	-	63
J	Pd/TiO_2 (P25)	Furfural vapor/water	400	1.01	98	30 (NR)[b]	-	-	-	28	-	41 (NR)[c,e]	33
K	0.1%Au/TiO_2 (Anatase)	FUR/water	160	40	100	10,800 (60)[b]	-	-	-	-	-	99 (NR)[c]	10

X is % conversion of furfural; NR is not reported or unable to calculate; Amb15 is Amberlyst-15

[a], Time on stream (TOS) for continuous systems

[b], () is W/F (g-cat/g-furfural*min) in continuous process

[c], () TOF, h^{-1} for product; (NR) TOF not reported or not enough information to calculate

[d], 1,4-pentanediol

[e], mixture of cyclopentanone, cyclopentanol, and 2-cyclopentenone – note 16% furan also produced

FA: Furfuryl Alcohol; THFA: tetrahydrofurfuryl alcohol; 2MF: 2-methylfuran; 2MTHF: 2-methyltetrahydrofuran; CP: cyclopentanone; 5H2P, 5-hydroxy-2-pentanone; 14PD, 1-4-pentanediol

CPME: cyclopentyl methyl ether; EtOAc: ethyl acetate

Conclusions

Pd-TiO_2/CACM catalyst demonstrated weak acid sites due to TiO_2 and medium acid sites due to mineral binders in the carbon catalyst support. The presence of weak acid sites and reduction in medium to strong acid sites with Ti doping of Pd on the ACM, promoted furan ring opening and increased the yield and selectivity of 5H2P, and reduced side reactions (e.g., humins) as evidenced by the higher carbon closures. A furfural hydrogenation/dehydration pathway forming 2MF was also evident, possibly due to partial segregation of Pd and Ti particles (indicated by SEM-EDS and H_2-TPR analysis). To the best of our knowledge, for the first time, a large space time yield of 134 g/Lcat/h (610 g/kg/h) and 39% selectivity of 5H2P from furfural was achieved using Pd-TiO_2/AC (LHSV 7.9 h^{-1}) in a continuous manner. The Pd-Cu and Pd-Fe catalysts demonstrated only medium to strong acid sites in catalyst structure and showed selectivity towards FA and THFA. The second metal (e.g., Cu) reduced over hydrogenation/dehydration to 2MF and resulted in a large STY of 259 g/Lcat/h and 42% selectivity of furfuryl alcohol for the Pd-Cu catalyst at 180 °C and 300 psig. Such positive results (i.e., selectivity changed to 5H2P in a continuous process generating large STY's), indicate it would be valuable to synthesize the catalyst in monolith form (Pd-TiO_2/activated carbon monolith) with better distribution and interaction of Ti with Pd, and perform time on stream studies to understand longevity, mass transfer effects at different gas/liquid flow ratios, and develop a kinetic model of furfural hydrogenation for scale-up purposes.

ASSOCIATED CONTENT

Supporting Information

The following results are presented, 1) equations for kinetic parameters, 2) FTIR analysis of base material, 3) XRD analysis, 4) BJH, BET, and t-plots, 5) effect of temperature and pressure on product selectivity and space time yield, 6) furfural conversion and carbon closure, 7) turnover frequency plots, 8) reaction pathway.

ACKNOWLEDGEMENTS

Support for this research and Maryam Pirmordi's PhD in Biochemical Engineering was provided by a USDA-NIFA Grant (Carbon Monolith Catalysts from Wood for Biobased Platform Chemicals: 2017-67021-26136). Authors acknowledge and thank Sarada Sripada for her contributions to FTIR analysis.

References

1. Y. Nakagawa, M. Tamura, K. Tomishige, *ACS Catal.* 2013, 3, 2655−2668.
2. M. Hronec, K. Fulajtarová, *Catal.Commun.* **2012,** *24*, 100-104.
3. R.M. Mironenko, V.P. Talsi, T.I. Gulyaeva, M.V. Trenikhin, O.B. Belskaya, *React. Kinet. Mech. Cat.* **2019,** *126* (2), 811-827.
4. S. Szymkuć, E.P. Gajewska, K. Molga, A. Wołos, R. Roszak, W. Beker, M. Moskal, P. Dittwald, B. Grzybowski, ChemRxiv. 2020. doi.org/10.26434/chemrxiv.12026439.v1 (these are preliminary reports that have not been peer-reviewed)
5. J. Heller, J. Barr, S. Ng, H.-R. Shen, R. Gurny, K. Schwach-Abdelaoui, A. Rothen-Weinhold, M. van de Weert, *J. Control. Release* **2002,** *78* (1-3), 133-141.
6. F. Liu, Q. Liu, J. Xu, L. Li, Y.-T. Cui, R. Lang, L. Li, Y. Su, S. Miao, H. Sun, B. Qiao, A. Wang, F. Jérôme, T. Zhang, *Green Chem.*, 2018, 20, 1770
7. G. Piancatelli, A. Scettri, S. Barbadoro, *Tetrahedron Lett.* **1976,** *17* (39), 3555-3558.
8. M. Hronec, K. Fulajtarová, T. Liptaj, *Appl. Cataly. A Gen.* **2012,** *437*, 104-111.
9. Y. Yang, Z. Du, Y. Huang, F. Lu, F. Wang, J. Gao, J. Xu, *Green Chem.* **2013,** *15* (7), 1932-1940.
10. G.-S. Zhang, M.-M Zhu, Q. Zhang, Y.-M. Liu, H.-Y. He, Y. Cao, *Green Chem.* **2016,** *18* (7), 2155-2164.
11. J. Ohyama, R. Kanao, A. Esaki, A. Satsuma, *Chem. Commun. (Camb)* **2014,** *50* (42), 5633-6.
12. J. Ohyama, R. Kanao, Y. Ohira, A. Satsuma, *Green Chem.* **2016,** *18* (3), 676-680.
13. R. Fang, H. Liu, R. Luque, Y. Li, *Green Chem.* **2015,** *17* (8), 4183-4188.
14. K. Fulajtárova, T. Soták, M. Hronec, I. Vávra, E. Dobročka, M. Omastová, *Appl. Cataly. A Gen.* **2015,** *502*, 78-85.
15. L. Liu, H. Lou, M. Chen, *Int. J. Hydrog. Energy* **2016,** *41* (33), 14721-14731.

16. S.T. Thompson, H.H. Lamb, *ACS Catal.* **2016,** *6* (11), 7438-7447.

17. Y. Yang, Z. Du, Y. Huang, F. Lu, F. Wang, J. Gao, J. Xu, *Green Chem.* **2013,** *15* (7), 1932-1940.

18. M. Hronec, K. Fulajtárová, I. Vávra, T. Soták, E. Dobročka, M. Mičušík, *Appl. Cataly. B Environ.* **2016,** *181*, 210-219.

19. S. Li, Y. Wang, L. Gao, Y. Wu, X. Yang, P. Sheng, G. Xiao, *Micropor. Mesopor. Mat. 262 (2018) 154–165.*

20. J. Lee, Y-T. Kim, G.W. Huber, *Green Chem.*, 2014, 16, 708–718.

21. Y. Cheng, H. Pham, J. Huo, R. Johnson, A.K. Datye, B. Shanks, *Mol. Catal.* 477 (2019) 110546.

22. Y. Tang, S. Cao, Y. Chen, T. Lu, Y. Zhou, L. Lu, J. Bao, *Appl. Surf. Sci.* 256 (2010) 4196–4200.

23. J. Du, J. Zhang, Y. Sun, W. Jia, Z. Si, H. Gao, X. Tang, X. Zeng, T. Lei, S. Liu, *J. Catal.* **2018,** *368*, 69-78.

24. Rodiansono, M.D. Astuti, T. Hara, N. Ichikuni, S. Shimazu., *Green Chem.* 2019, 21, 2307–2315.

25. R. Gérardy, D.P. Debecker, J. Estager, P. Luis, J-C. M. Monbaliu. *Chem. Rev.* 2020. https://dx.doi.org/10.1021/acs.chemrev.9b00846

26. C. Xu, E. Paone, D. Rodrı´guez-Padro´n, R. Luque, F. Mauriello., *Chem. Soc. Rev.,* 2020, 49, 4273--4306.

27. Y.Wang, D. Zhao, D. Rodríguez-Padrón, C. Len., *Catalysts* 2019, 9, 796; doi:10.3390/catal9100796

28. Y. Wang, P. Prinsen, K.S. Triantafyllidis, S.A. Karakoulia, P.N. Trikalitis, A. Yepez, C. Len, R. Luque, *ACS Sustain. Chem. Eng.* 6 (2018) 9831−9844.

29. A.J. Garcia-Olmo, A. Yepez, A.M. Balu, P. Prinsen, A. Garcia, A. Maziere, C. Len, R. Luque, *Tetrahedron* 73 (2017) 5599-5604.

30. P. Liu, W. Qiu, C. Zhang, Q. Tan, C. Zhang, W. Zhang, Y. Song, H. Wang, C. Li, *ChemCatChem* 11 (2019) 3296–3306.

31. N.S. Biradar, A.A. Hengne, S.N. Birajdar, R. Swami, C.V. Rode., *Org. Process Res. Dev.* 2014, 18, 1434−1442

32. J. Zhu, Y. Jia, M. Li, M. Lu, J. Zhu, *Ind. Eng. Chem. Res.* 52 (2013) 1224−1233.

33. T. Omotoso, L.V. Herrera, T. Vann, N.M. Briggs, L.A. Gomez, L. Barrett, D. Jones, T. Pham, B. Wang, S.P. Crossley., *Appl. Catal. B Environ*. 254 (2019) 491–499

34. J. Weber, A. Thompson, J. Wilmoth, R.J. Gulotty Jr, J.R. Kastner, *Energy Fuels* **2017,** *31* (9), 9529-9541.

35. A.H. El-Sheikh, A.P. Newman, H. Al-Daffaee, S. Phull, N. Cresswell, S.York, *Surf. Coat. Technol.* **2004,** *187* (2-3), 284-292.

36. M.L. Toebes, J.A. van Dillen, K.P. de Jong, *J. Mol. Catal. A Chem.* **2001,** *173* (1-2), 75-98.

37. J. De Boer, B. Linsen, T. Van der Plas, G. Zondervan, *J. Catal.* **1965,** *4* (6), 649-653.

38. M. Pirmoradi, N. Janulaitis, R.J. Gulotty Jr., J.R. Kastner, *ACS Omega* 2020, 5, 14, 7836–7849

39. J.C. Yori, J.M. Grau, V. M. Benı´tez, J. Sepu´lveda., *Appl. Catal. A Gen.* 286 (2005) 71–78.

40. R. Yang, G. Li, C. Hu, *Catal. Sci. Technol.* **2015,** *5* (4), 2486-2495.

41. F. Bossola, X.I. Pereira-Hernández, C. Evangelisti, Y. Wang, V. Dal Santo, *J. Catal.* **2017,** *349*, 75-83.

42. G. Busca, *Phys. Chem. Chem. Phys.* **1999,** *1* (5), 723-736.

43. D. Topaloğlu Yazıcı, C. Bilgic, *Surf. Interface Anal.* **2010,** *42* (6-7), 959-962.

44. M. Pirmoradi, N. Janulaitis, R.J. Gulotty Jr., J.R. Kastner, Bi-metal Supported Activated Carbon Monolith Catalysts for Selective Hydrogenation of Furfural, In Review. 2020 *Industrial & Engineering Chemistry Research.*

45. S. Biniak, R. Diduszko, W. Gac, M. Pakuła, A. Świątkowski, *React. Kinet. Mechan. Catal.*. **2010,** *101* (2), 331-342.

46. A. Śrębowata, W. Lisowski, J.W. Sobczak, Z. Karpiński, *Catal. Today* **2011,** *175* (1), 576-584.

47. C. Espro, B. Gumina, E. Paone, F. Mauriello, *Catalysts* **2017,** *7* (3), 78.

48. W.-J. Shen, M. Okumura, Y. Matsumura, M. Haruta, *Appl. Catal. A Gen.* **2001,** *213* (2), 225-232.

49. M. Gurrath, T. Kuretzky, H. Boehm, L. Okhlopkova, A. Lisitsyn, V. Likholobov, *Carbon* **2000,** *38* (8), 1241-1255.

50. R. Prins, *Chem. Rev.* 2012, 112, 2714−2738

51. S. Riyapan, Y. Boonyongmaneerat, O. Mekasuwandumrong, P. Praserthdam, J. Panpranot., *Catal. Today* 245 (2015) 134–138.

52. J. Xu, K. Sun, L. Zhang, Y. Ren, X. Xu. *Catal. Comm.* 6 (2005) 462–465.

53. Pinna, F.; Menegazzo, F.; Signoretto, M.; Canton, P.; Fagherazzi, G.; Pernicone, N., *Appl. Catal. A Gen.* **2001,** *219* (1-2), 195-200.

54. J. Weber, A. Thompson, J. Wilmoth, R.J. Gulotty, Jr., J.R. Kastner. *Energy Fuels* 2017, 31, 9529−9541

55. I.I. Salame, T.J. Bandosz, Surface Chemistry of Activated Carbons: *J. Colloid Interface. Sci.* 2001, 240, 252−258.

56. R. Mane, S. Patil, M. Shirai, S. Rayalu. C. Rode, *Appl. Catal.B Environ.* 2017, 204, 134–146.

57. X. Zheng, N. Yu, X. Wang, Y. Wang, L. Wang, X. Li, X. Hu. *Sci. Rep.* (2018) 8:6463

58. D.R. Vardon, A.E. Settle, V. Vorotnikov, M.J. Menart, T.R. Eaton, K.A. Unocic, K.X. Steirer, K.N. Wood, N.S. Cleveland, K.E. Moyer, W.E. Michener, G.T. Beckham, *ACS Catal.* 2017, 7, 6207−6219.

59. M-Y. Kim, Y. San You, H-S. Han, G. Seo., *Catal. Lett.* (2008) 120:40–47

60. P. Sudarsanam, H. Li, T.V. Sagar. TiO_2-Based Water-Tolerant Acid Catalysis for Bio-Derived Fuels and Chemicals. *ACS Catal.*, Just Accepted Manuscript, DOI: 10.1021/acscatal.0c01680, Publication Date (Web): 20 Jul 2020

61. C.-Y. Liu, R.-P. Wei, G.-L Geng, M.-H. Zhou, L.-J. Gao, G.-M. Xiao, *Fuel Process. Technol.* **2015,** *134*, 168-174.

62. S. Liu, Y. Amada, M. Tamura, Y. Nakagawa, K. Tomishige, *Green Chem.* **2014,** *16* (2), 617-626.

63. Q. Liu, B. Qiao, F. Liu, L. Zhang, Y. Su, A. Wang, T. Zhang., *Green Chem*., 2020, 22, 3532–3538

64. J.-P. Lange, R. Price, P.M. Ayoub, J. Louis, P. Petrus, L. Clarke, H. Gosselink, *Angew. Chem. Int. Ed.* 2010, 49, 4479 –4483.

65. J.-A.T. Schwartz, Ru,Re/Carbon Catalyst for Hydrogenation in Aqueous Solution. E.I. Du Pont de Nemours and Company US Pat., 5 478 952, 1995.

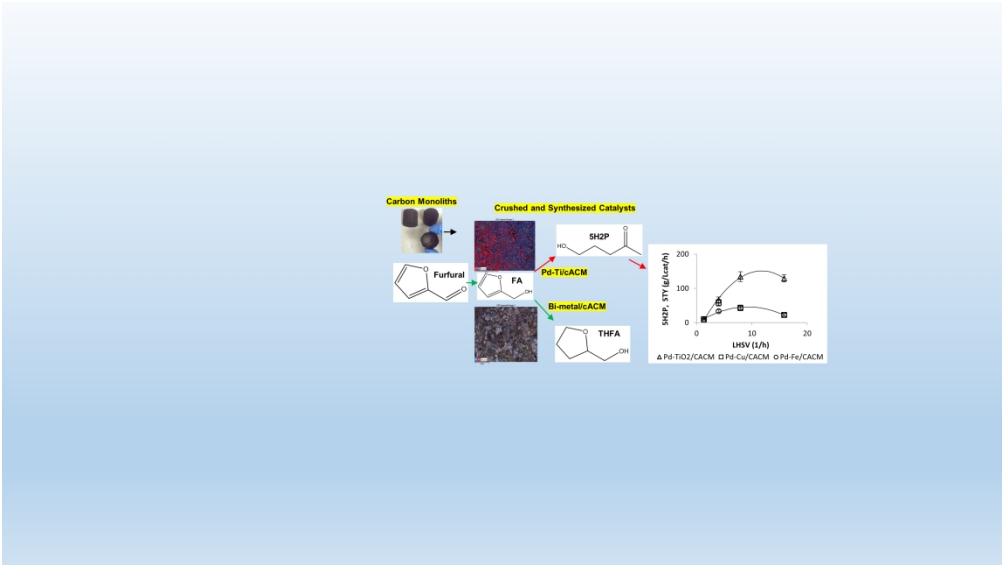

338x190mm (300 x 300 DPI)